Atmospheric Environment 247 (2021) 118203

Contents lists available at ScienceDirect

Atmospheric Environment

journal homepage: http://www.elsevier.com/locate/atmosenv

Identification of potential sources of elevated $PM_{2.5}$-Hg using mercury isotopes during haze events

Yue Qiu [a,e], Pengxue Gai [b], Fange Yue [a], Yuanyuan Zhang [b], Pengzhen He [a], Hui Kang [a], Xiawei Yu [a], Paul K.S. Lam [c], Jiubin Chen [b,**], Zhouqing Xie [a,d,*]

[a] Department of Environmental Science and Engineering, University of Science and Technology of China, Hefei, 230026, China
[b] Institute of Surface-Earth System Science, Tianjin University, Tianjin, 300072, China
[c] Department of Chemistry, State Key Laboratory of Marine Pollution, City University of Hong Kong, Hong Kong, China
[d] Center for Excellence in Urban Atmospheric Environment, Institute of Urban Environment, Chinese Academy of Sciences, Xiamen, 361021, China
[e] Suzhou Institute for Advanced Study, University of Science and Technology of China, Suzhou, 215123, China

HIGHLIGHTS

- $\Delta^{199}Hg_{PBM}$ together with 3D model is powerful tool to trace sources of $PM_{2.5}$-Hg.
- Sources and transport of $PM_{2.5}$-Hg during haze are complex for different seasons.
- Biomass burning had an important contribution to $PM_{2.5}$-Hg in Beijing in winter.
- $\Delta^{200}Hg_{PBM}$ may be caused by photoreactions on the anthropogenic-emission particles.

GRAPHICAL ABSTRACT

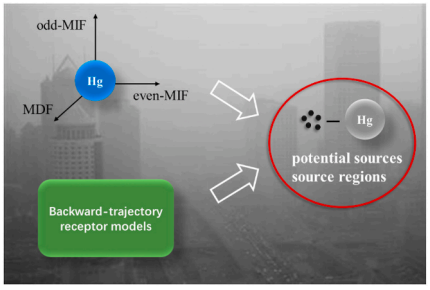

ARTICLE INFO

Keywords:
Hg isotopes
Backward trajectory
Particle-bound Hg
Haze

ABSTRACT

Atmospheric mercury (Hg) pollution has become a serious problem in megacities. In this study, we applied Hg isotopes together with backward-trajectory receptor models to investigate the potential sources and transport of elevated $PM_{2.5}$-Hg during two haze events in autumn (Oct. and Nov. in 2014) and winter (Jan. in 2015). Results showed that the sources and transport patterns of $PM_{2.5}$-Hg during haze are complex for different seasons. In autumn, the dominant sources were local and/or regional anthropogenic emissions from northern China, whereas the long-range transport contribution of biomass burning originated from northeastern China in 2014 and eastern China in 2015. Notably, the biomass burning from northeastern China served as an important contribution to elevated $PM_{2.5}$-Hg in winter. Our data set also suggested that the $\Delta^{200}Hg_{PBM}$ values may be due to heterogeneous photoreactions on the particles emitted by coal burning, smelting, and cement production, along with photooxidation from the upper troposphere, and could be used as a potential indicator of particle-bound mercury sources owing to its contribution to the exhibited variability. Hg isotopes, together with meteorological models, could be employed to trace the sources of particle-bound Hg in the atmosphere. This study provides a new way to explore the potential sources of atmospheric particulate mercury and its vectors during haze evolution.

* Corresponding author. Department of Environmental Science and Engineering, University of Science and Technology of China, Hefei, 230026, China.
** Corresponding author.
E-mail addresses: jbchen@tju.edu.cn (J. Chen), zqxie@ustc.edu.cn (Z. Xie).

https://doi.org/10.1016/j.atmosenv.2021.118203
Received 22 August 2020; Received in revised form 9 December 2020; Accepted 6 January 2021
Available online 9 January 2021

1. Introduction

Atmospheric Hg exists primarily in three forms with different physical and chemical properties: gaseous elemental Hg (GEM), gaseous oxidized Hg (GOM), and particle-bound Hg (PBM) (Selin, 2009). GEM is the most abundant Hg species in the atmosphere, which accounts for approximately 90% of the total Hg. Since GEM is chemically stable, it can be transported long distances on a global scale. The residence time of GOM in the atmosphere is relatively short, and it is easily removed from the atmosphere by adsorption onto particles or dissolution in raindrops before deposition onto the earth's surface. PBM is mainly composed of Hg^{2+} and also contains a small amount of Hg^0. Because the residence time of PBM in the atmosphere is short, PBM can only be transported at regional or local scales, which can reflect the Hg pollution and short-term cycle of local emission sources (Selin, 2009; Subir et al., 2012). PBM is considered to be contributed by multiple sources, and it will undergo complex transformation processes during transport in the atmosphere (Subir et al., 2012). PBM, especially fine-particle-bound Hg (e.g., $PM_{2.5}$-Hg) may pose a direct threat to the health of humans through respiration in megacity areas (Cui et al., 2020; Liang et al., 2019). Moreover, PBM may be converted into more toxic organic forms (e.g. MeHg) upon settling to the surface (especially the aqueous surface), endangering human beings and other organisms in the ecosystem (Maher et al., 2020). Therefore, potential sources of PBM should be studied to improve the understanding of atmospheric mercury cycle networks.

The isotope approach could be used to trace Hg sources and transformation in the atmosphere. Hg has seven isotopes, namely, ^{196}Hg, ^{198}Hg, ^{199}Hg, ^{200}Hg, ^{201}Hg, ^{202}Hg, and ^{204}Hg. The transport and transformation of Hg under natural and anthropogenic conditions can induce three types of Hg isotopic fractionation, including the mass-dependent fractionation (MDF, including $\delta^{202}Hg$), the odd-mass-number mass-independent fractionation (odd-MIF, including $\Delta^{199}Hg$ and $\Delta^{201}Hg$), and the even-mass-number mass-independent fractionation (even-MIF, including $\Delta^{200}Hg$ and $\Delta^{204}Hg$) (Bergquist and Blum, 2007; Chen et al., 2012; Gratz et al., 2010; Hintelmann and Lu, 2003; Sherman et al., 2012). Although many physical and chemical processes lead to MDF (Bergquist and Blum, 2007; Estrade et al., 2009; Kritee et al., 2007; Janssen et al., 2016; Smith et al., 2015; Wiederhold et al., 2010), large values of odd-MIF occur only through photochemical reactions, including photoreduction (Bergquist and Blum, 2007; Rose et al., 2015; Sherman et al., 2010; Zheng and Hintelmann, 2009, 2010), photodemethylation (Bergquist and Blum, 2007), and photooxidation (Sun et al., 2016). Even-MIF primarily signifies wet deposition; in some studies, it is assumed to represent the contribution of Hg that is transported a long distance from the upper troposphere to the surface; however, the formation mechanism of even-MIF remains unclear (Cai and Chen, 2016; Chen et al., 2012). Moreover, according to previous studies, $\Delta^{199}Hg$ has a wide variation in PBM samples. Relatively higher (up to 1.16‰) and lower (up to −1.00‰) $\Delta^{199}Hg$ might indicate the contributions of long-range transport and biomass burning, respectively (Carignan et al., 2009; Chen et al., 2012; Demers et al., 2013; Jiskra et al., 2015; Wang et al., 2015; Yin et al., 2013; Yuan et al., 2015). In addition, the $\Delta^{199}Hg$ of PBM formed by anthropogenic emissions generally would be negative or close to zero (Sun et al., 2013, 2014). Therefore, Hg is a unique heavy metal with "three-dimensional" isotope systems, indicating that Hg isotopes could be used to identify the potential sources of Hg pollution.

China is the largest developing country in the world. Owing to its rapid economic development, China has become the largest energy consumer on the planet and suffers from serious atmospheric Hg pollution (especially in urban areas) (Fu et al., 2012; Teng et al., 2020; Zhang et al., 2015). Pacyna et al. (2006) suggested that burning fossil fuel is the largest single anthropogenic emission source of Hg in the atmosphere. In addition, industrial activities, including nonferrous metal smelting and cement production in China, also release large amounts of Hg into the atmosphere (Zhang et al., 2015). Duan et al. (2016) investigated the chemical species PBM in $PM_{2.5}$ in Shanghai and found that the carbonaceous composition may affect the transformation of Hg in the atmosphere. Long-term continuous measurements of atmospheric Hg species were conducted by Hong et al. (2016), which revealed that atmospheric Hg pollution on hazy days was mainly caused by local emissions, with limited contribution from long-range transport.

Other studies have also addressed the sources of aerosol PBM and the processes it undergoes in the megacity Beijing, which has both a large industrial system and large population and experiences serious air pollution issues throughout the year, especially in autumn and winter. Huang et al. (2016) first studied the sources and photoreaction of annual $PM_{2.5}$-Hg collected in Beijing using Hg isotopes. By comparing the range of $\Delta^{199}Hg$ between the source materials and $PM_{2.5}$ samples, coal combustion was found to be the dominant anthropogenic emission source in winter, whereas biomass burning contributed a significant fraction in autumn. However, Huang et al. (2019) suggested that photoreduction may modify the Hg isotope signatures of PBM and cause a diel variation of odd-MIF, such as $\Delta^{199}Hg_{PBM}$ and $\Delta^{201}Hg_{PBM}$, in $PM_{2.5}$ samples. This indicates a possible transformation of PBM when transported from emission source regions to sampling sites and renders source identification more difficult. These results indicate the need for further systematic study to better identify the sources of $PM_{2.5}$-Hg and the impact of the PBM transformation along the transmission path. On the basis of these previous findings, the goal of this study was to use Hg isotopes, along with backward-trajectory receptor models that have not yet been employed in this region, despite the useful information they could ultimately provide, to further identify the potential sources and source regions of $PM_{2.5}$-Hg during haze periods which lasted for several days.

2. Materials and methods

2.1. Sampling location and sample collection

The locations of the sampling sites are shown in Fig. 1. The $PM_{2.5}$ samples were collected during autumn and winter haze events in Beijing using a $PM_{2.5}$ high-volume air sampler (Wuhan Tianhong Instrument Co., Ltd.), which collected particles at a flow rate of 1.05 m^3 min^{-1} through a size-selective $PM_{2.5}$ inlet on a pre-combusted (450 °C for 6 h) quartz fiber filter (Quartz Microfiber Filters, 203 mm × 254 mm, 25 sheets, CAT No. 1851-865, Lot No. 9730862, UK). We collected samples from two haze periods in Beijing during the period of October 2014 to January 2015, with the weather of the sampling time listed in Table S1. The aerosol samples were placed in a freezer (−4 °C) for storage. The collection duration of each aerosol sample was 12 h in this study.

2.2. Hg concentration and isotope analysis

In this study, aerosol samples were pretreated according to the method reported in Huang et al. (2015). The pyrolysis device consisted of two muffle furnaces—one could heat to as high as 900 °C (combustion furnace) while the other maintained a constant temperature of 900 °C (decomposition furnace). Each filter sample was placed in a short quartz tube, which was then placed inside a long quartz tube located in the pyrolysis device before the commencement of the pyrolysis process. The PBM attached to the filter would be transferred to the absorption solution (50% v/v HNO_3; HCl = 2:1, 5 mL) through the purging of high-purity oxygen gas. After the pyrolysis process, the absorption solution in the bubbler tube was diluted to 10 mL and transferred to a polyborosilicate glass bottle. The addition of 0.1% BrCl (v/v) was then

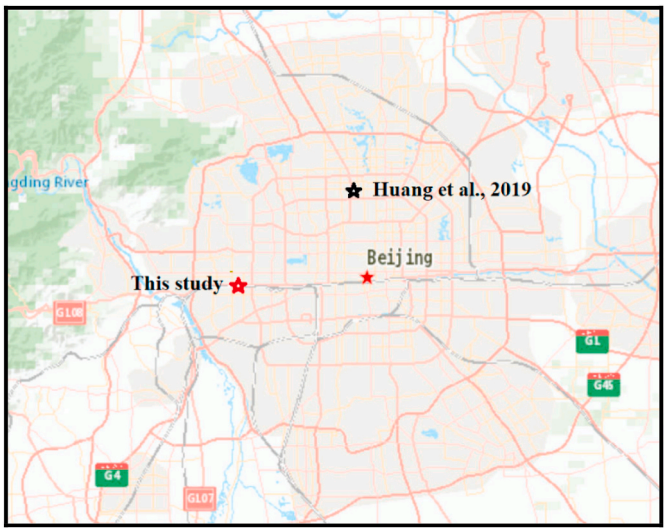

Fig. 1. Schematic diagram of sampling sites. The sampling site of this study was located at the Chinese Academy of Sciences University Yuquan Rd Campus, Beijing, China (represented by the hollow red pentagram). The sampling site in Huang et al. (2019) was located at the Institute of Atmospheric Physics, Chinese Academy of Sciences, Beijing, China (represented by the hollow black pentagram). The map was provided by ArcGIS. (For interpretation of the references to color in this figure legend, the reader is referred to the Web version of this article.)

performed to prevent the loss of PBM during storage. Sample bottles were sealed with sealing film and saved at 4 °C for the measurement of Hg content and Hg stable isotopes. The Hg content of all aerosol samples was determined using a Tekran 2500 monitor (Model 2500 Cold Vapor Atomic Fluorescence Spectrophotometry detector, Tekran Instruments, USA) according to the EPA1631e method, with a precision generally better than 10%. Standards including GSS-5 (yellow red soil), Trace Metals–Loamy Sand 1, and GSD-11 (stream sediments) were used as certified reference materials in the measurement of Hg content and measured regularly for quality control. In terms of experimental blanks, we measured the Hg amount in each gold capture tube (a total of 11 tubes) after the same procedures as sample determination (procedural blanks). Results showed that the average Hg amount of the procedural blanks was 1.15 ± 0.91 pg (mean ± 2 SD), which was not more than 0.1‰ of the Hg amount in each $PM_{2.5}$ sample. Moreover, the Hg amount of two quartz fiber filters which sampled 1 min during non-haze days was also measured (sampling blanks) to estimate the effect of sample matrix on Hg isotope determination. The average Hg amount of the sampling blanks was 0.39 ± 0.14 ng (mean ± 2 SD), which was not more than 4% of the Hg amount in each $PM_{2.5}$ sample. After calculation, we concluded that the effect of sample matrix on Hg isotope determination can be negligible. The detailed calculation is shown in Table S3.

In this study, five stable Hg isotopes (^{198}Hg, ^{199}Hg, ^{200}Hg, ^{201}Hg, and ^{202}Hg) were measured in the aerosol samples collected using an MC-ICP-MS (Neptune Plus, ThermoFisher, USA) at the State Key Laboratory of Environmental Geochemistry, Institute of Geochemistry, China. Previous studies provided details of the analytical procedures and instrumental parameter settings (Huang et al., 2015; Wang et al., 2015; Yuan et al., 2015).

The mass-dependent fractionation (MDF) of Hg isotopes is reported in delta notation (δ) in units of per mil, referenced to the bracketed NIST 3133 Hg standard, which is expressed as

$$\delta^{xxx}Hg\ (‰) = ([(^{xxx}Hg/^{198}Hg)_{sample}/(^{xxx}Hg/^{198}Hg)_{NIST3133}] - 1) \times 1000$$

where xxx = 199, 200, 201, and 202. Any isotope composition that did not follow the theoretical MDF was considered to be an isotope anomaly caused by MIF. MIF values are indicated by "capital delta (Δ)" notation (in per mil) and are predicted from $\delta^{202}Hg$ using the MDF law:

$$\Delta^{xxx}Hg = \delta^{xxx}Hg - \beta^{xxx} \times \delta^{202}Hg$$

where the mass-dependent scaling factor β^{xxx} is 0.252 for ^{199}Hg, 0.502 for ^{200}Hg, 0.752 for ^{201}Hg, and 1.493 for ^{204}Hg.

For quality assurance and control, we used NIST SRM 3177 Hg as a secondary standard and performed multiple analyses during each sample analysis session. The ranges of the Hg isotopes of NIST SRM 3177 Hg led to average $\delta^{202}Hg$, $\Delta^{199}Hg$, $\Delta^{200}Hg$, and $\Delta^{201}Hg$ values of −0.56‰ ± 0.16‰, 0.01‰ ± 0.08‰, 0.02‰ ± 0.07‰, and −0.02‰ ± 0.10‰, respectively (2 SD, n = 11). Because the reference material UM-Almaden was no longer being produced and the Hg isotopic compositions of UM-Almaden and NIST SRM 3177 Hg were strictly the same, we could compare the measurement data of NIST SRM 3177 Hg from this study with those from previous studies (Bergquist and Blum, 2007; Chen et al., 2010; Huang et al., 2015, 2016, 2019). The values in this study were found to be consistent with those from previous results. Owing to the limited sample amount available, each sample was measured only once. Given this, we used the uncertainty of the Hg isotopes of NIST SRM 3177 Hg to represent the uncertainty of the isotopic composition of the aerosol samples.

2.3. Organic/elemental carbon (OC/EC), heavy metals and water-soluble K^+ analysis

According to previous studies, organic compounds had an important impact on adsorption of Hg species to particles (Archer and Blum, 2018). In this study, a punch of each filter was prepared to determine the contents of organic and elemental carbon through Multiwavelength Carbon Analyzer (DRI Model, 2015; Desert Research Institute, USA). Besides coal combustion, nonferrous metal production and cement production also were important anthropogenic emission sources in global scale (Table S6). In this study, the contents of eight heavy metals (Cd, Co, Cr, Cu, Mn, Ni, Pb, Zn) in the aerosol samples were measured using ICP-MS (NexION, 2000C, PerkinElmer, USA) to estimate the contributions of these emission sources. The measurement data are listed in Table S4.

According to previous studies, biomass burning inputs large amounts of particulate matter into the troposphere and plays an important role in the severe haze pollution in China (Andreae, 2019; Cheng et al., 2013; Wang et al., 2020); meanwhile, the global PBM emission supply does not include biofuel production and combustion. Previous studies have found that water-soluble K^+ is a good indicator of the contribution of biomass burning (Cheng et al., 2013; Dibb et al., 1996). For each $PM_{2.5}$ sample, four punches of each filter were put into a colorimetric tube, added Milli-Q water (≥18 MΩ) to 10 mL. Through ultrasonic vibration for 30 min, water-soluble ions on the filter were transferred to the colorimetric tube. Then, the liquid in the test tube was pumped into another clean colorimetric tube through pre-washed 0.22-μm filters. Ultrasonic vibration and filtration steps were repeated again to ensure that water-soluble ions were completely removal from the filter. Finally, the colorimetric tube (20 mL) was shook well and the liquid was poured into the sample-injected tube of ion chromatography. In this study, the contents of water-soluble K^+ in the aerosol samples were measured using ion chromatography (ICS-2100, ThermoFisher, USA). Each batch of test had at least two reagent blanks, two field blanks, and one recovery. The recovery rate of all recovered samples was between 90% and 110%. The typical analytical precision of the instrument was better than 10% relative standard deviation (RSD) for all ions (Chen et al., 2016). The measurement data are listed in Table S5.

2.4. Air-mass backward trajectory analysis

In this study, TrajStat geographical-information-system-based software and gridded meteorological data (Global Data Assimilation

System, GDAS1) from the U.S. National Oceanic and Atmospheric Administration were used to calculate 120-h backward trajectories of air masses arriving at a height of 50 m above ground level at the sampling sites, which represented air masses within the haze boundary layer (Cheng et al., 2015; Fu et al., 2019). The duration time of the trajectories was selected to investigate the regional and long-range transport patterns that may have influenced the PBM isotopic compositions. In this study, a method for investigating the link between atmospheric transport patterns and PBM isotopic compositions was utilized to access the contributions of anthropogenic emission sources to PBM isotopic compositions through a combined analysis between backward trajectory receptor models and the Hg isotopic compositions of aerosol samples (Fu et al., 2019). The cumulative anthropogenic PBM emission (∑PBM emission) of each PBM sample was calculated by summing all the gridded emissions of the grids encountered by the air mass transported during the past five days based on the Arctic Monitoring and Assessment Programme (AMAP)/United Nations Environment Programme (UNEP) gridded PBM emission inventory of 2010 (AMAP/UNEP, 2013; Fu et al., 2019). The fractional ∑PBM emission was defined as the percentage of ∑PBM emission over a selected geographic region (Figure S1) relative to the total ∑PBM emission. Due to the statistical incompleteness of anthropogenic emission data in areas aboard according to global Hg emission dataset, the "long-range transport" was used to represent the contribution of anthropogenic PBM emissions from areas aboard when we discussed the correlations between fractional ΣPBM emission of different regions and $\Delta^{199}Hg_{PBM}$.

3. Results and discussion

Previous studies usually regard a 75 μg/m^3 of $PM_{2.5}$ content as an important standard for identifying and partitioning haze events (Zheng et al., 2016; Yang et al., 2020). Therefore, in this study, we defined a sampling day with more than 75 μg/m^3 in $PM_{2.5}$ content as a hazy day. In addition, we gave a definition to a single haze event in a narrow sense, which was considered to be a period when the $PM_{2.5}$ content from above 75 μg/m^3 to below 75 μg/m^3. The contents of PBM and Hg isotope ratios are listed in Table S2. The ranges of Δ^{199}Hg, Δ^{200}Hg, and δ^{202}Hg in our 13 $PM_{2.5}$ samples ranged from −0.85‰ to 0.15‰, from 0.00‰ to 0.08‰, and from −1.30‰ to −0.15‰, respectively. To make a comparative study, the Hg isotope data of Huang et al. (2019), which comprise 56 $PM_{2.5}$ samples continuously collected in autumn (Sept. and Oct. of 2015) in Beijing, 17 of which collected during haze and 3 of which collected during non-haze were compiled for analysis (3 non-haze samples together with 8 haze samples consisted a single haze event due to the continuity of sampling time). The ranges of Δ^{199}Hg, Δ^{200}Hg, and δ^{202}Hg in the 17 $PM_{2.5}$ samples collected during haze were from −0.53‰ to 0.69‰, −0.02‰–0.14‰, and −1.21‰ to 0.52‰, respectively. By combining the data reported by Huang et al. (2019), we tried to identify the potential sources of elevated PBM in the haze period, along with determining the emission models. The total ΣPBM emission of each aerosol sample collected during the haze period could be calculated based on the grid data distribution of PBM anthropogenic emission sources (as shown in Fig. 2) combined with the backward trajectory of each sample; meanwhile, the fractional ΣPBM emission of each aerosol sample collected during the haze period was defined according to different geographic regions. Moreover, emissions from various sectors used in the dataset (Table S6) were listed in the global Hg assessment report (UNEP, 2013).

3.1. The impacts of multiple emission sources and photoreduction during transportation on Hg isotopes

According to previous studies, The δ^{202}Hg vs. Δ^{199}Hg could be used to identify sources effectively (Chen et al., 2012, 2016). Fig. 3a shows the δ^{202}Hg and Δ^{199}Hg in PBM collected during haze in this study and Huang et al. (2019), which are compared with those in typical

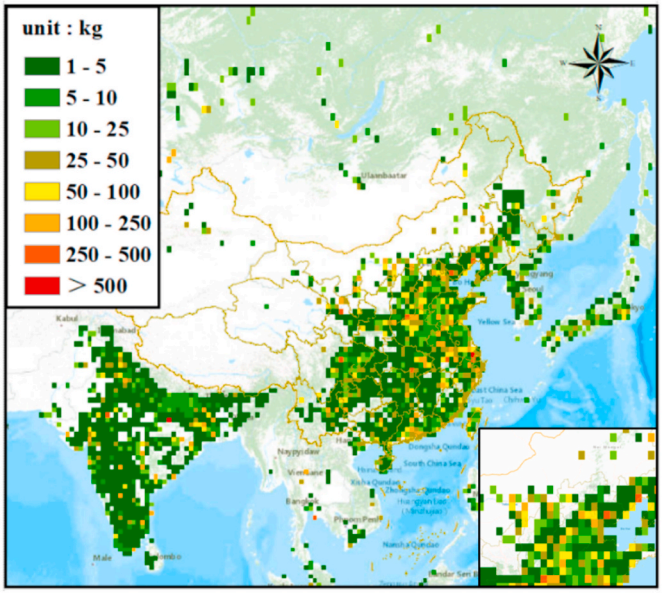

Fig. 2. Grid data distribution of PBM anthropogenic emission sources in eastern Asia in 2010 calculated from the global Hg assessment report, in which the PBM anthropogenic emission sources did not include anthropogenic biomass burning (AMAP/UNEP, 2013; UNEP, 2013). Grid data distribution of the PBM anthropogenic emission sources in northern China was displayed on bottom right corner. The emissions from various sectors are listed in Table S6 according to UNEP (2013).

anthropogenic emission sources (Huang et al., 2016) and biomass (Jiskra et al., 2015; Yin et al., 2013; Carignan et al., 2009). It is found that the δ^{202}Hg in PBM of all haze samples was within the range of typical anthropogenic emission sources, which may indicate the contributions of typical anthropogenic emission sources including coal combustion, cement production, nonferrous metal smelting, and urban soil and dust. The strong anthropogenic contribution may be also

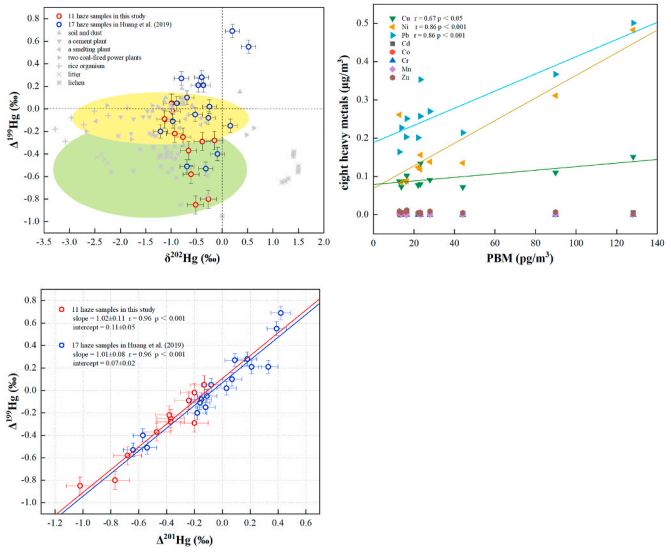

Fig. 3. (a) The δ^{202}Hg vs. Δ^{199}Hg in PBM collected during haze in this study and Huang et al. (2019), the uncertainty of each sample was expressed as 2 SD. The δ^{202}Hg vs. Δ^{199}Hg in typical anthropogenic emission sources (Huang et al., 2016) and biomass (Jiskra et al., 2015; Yin et al., 2013; Carignan et al., 2009) is added for comparison. **(b)** The correlations between the contents of PBM and eight heavy metals in $PM_{2.5}$ collected during haze in this study. **(c)** The Δ^{201}Hg vs. Δ^{199}Hg in PBM collected during haze in this study and Huang et al. (2019), the uncertainty of each sample was expressed as 2 SD.

supported by the relationships between Hg and other particulate components in $PM_{2.5}$. Fig. 3b shows the correlations between the contents of eight heavy metal elements and PBM content in 11 haze samples in this study, it is found that the contents of Cu, Ni, and Pb had a significant increase with a rise in PBM content. This may reflect the contributions of anthropogenic activities to elevated $PM_{2.5}$-Hg during haze again. Moreover, the significant negative Δ^{199}Hg in PBM of some haze samples, which could not be explained by anthropogenic emission sources, was within the range of biomass. Previous studies have reported that the burning process will not induce any MIF so that the signature of Δ^{199}Hg in biomass could be conserved (Sun et al., 2014; Huang et al., 2015). This may mean that biomass burning also have a contribution to elevated $PM_{2.5}$-Hg in these haze samples. As black carbon is one of the important products during biomass burning, here the distribution pattern of black carbon aerosol optical thickness (AOT) was used to identify the occurrence of biomass burning during haze (Figure S2). It was found that the black carbon AOT in northeastern China and eastern China had an obvious increase during haze, which may again indicate the possible contribution of biomass burning to PBM. However, the significant positive Δ^{199}Hg in PBM of some haze samples was out of the ranges of typical anthropogenic emission sources and biomass. Since large extents of odd-MIF occur mainly through photochemical reactions, it may suggest the contribution from MIF during atmospheric processes.

According to previous studies, the ratio of $\Delta^{199}Hg/\Delta^{201}Hg$ could be used to indicate different photochemical reactions (Bergquist and Blum, 2007; Sun et al., 2016). As shown in Fig. 3c, the ratios of $\Delta^{199}Hg/\Delta^{201}Hg$ in PBM collected during haze in this study and Huang et al. (2019) were 1.02 ± 0.11 ($r = 0.96$, $p < 0.001$) and 1.01 ± 0.08 ($r = 0.96$, $p < 0.001$), respectively, which were both close to the ratio of $\Delta^{199}Hg/\Delta^{201}Hg$ observed in photoreduction of Hg^{2+} in aqueous system (Bergquist and Blum, 2007). These results may indicate that the signatures of odd-MIF in PBM would be mainly impacted by photoreduction which occurred during transportation. Therefore, the isotopic compositions of PBM collected during haze were considered to be jointly impacted by multiple emission sources and photoreduction during transportation.

3.2. The impacts of situ photoreactions on mercury isotopic compositions of $PM_{2.5}$ samples during haze

According to Table 1, the content of PBM and mercury isotopic compositions of two non-haze $PM_{2.5}$ samples were compared with those of non-haze $PM_{2.5}$ samples reported by Huang et al. (2019). It was found that the content of PBM and mercury isotopic compositions of two non-haze $PM_{2.5}$ samples were within the range of those of non-haze $PM_{2.5}$ samples reported by Huang et al. (2019), which may indicate that $PM_{2.5}$-Hg collected in non-haze days had relatively similar sources. It was found that the odd-MIF of the two non-haze samples (GKD49 and GKD357) and non-haze samples reported by Huang et al. (2019) (Δ^{199}Hg: 0.20‰ ± 0.64‰, Δ^{201}Hg: 0.14‰ ± 0.54‰, mean ± 2 SD) was higher than the average value of that of $PM_{2.5}$ samples collected in haze days (Δ^{199}Hg: -0.34‰ ± 0.59‰, Δ^{201}Hg: -0.44‰ ± 0.55‰, mean ± 2 SD) in this study. According to previous studies, large positive values of odd-MIF occur mainly through photoreduction, which may indicate that $PM_{2.5}$-Hg collected in haze days was unlikely to be affected by situ photoreduction due to decline of refraction of UV in planetary boundary layer (PBL) (Chylek and Zhan, 1990). Moreover, the variation range of $\Delta^{200}Hg_{PBM}$ of $PM_{2.5}$ samples collected in haze days (0.03‰ ± 0.04‰, mean ± 2 SD) in this study was less than that of PM2.5 samples collected in non-haze days (0.14‰ ± 0.54‰, mean ± 2 SD) reported by Huang et al. (2019). According to previous studies, positive Δ^{200}Hg observed in precipitation samples (mainly Hg^{2+}) may indicate the contribution of photooxidation in the upper troposphere, which may mean that $PM_{2.5}$-Hg collected in haze days was unlikely to be contributed by vertical transportation of $PM_{2.5}$-Hg generated from photooxidation in upper atmosphere. Through analysis above, the impacts of situ photoreduction and photooxdiation on $PM_{2.5}$-Hg both were relatively weak during haze.

Table 1
This table is a comparison of the contents and isotopic compositions in PBM collected during haze and non-haze periods. The contents and isotopic compositions in PBM collected during haze periods were listed in this study, those of which collected during non-haze periods were listed in this study and Huang et al. (2019).

Sample ID	Hg con. (pg/m^3)	δ^{202}Hg (‰)	Δ^{199}Hg (‰)	Δ^{201}Hg (‰)	Δ^{200}Hg (‰)
GKD49	17.39	−1.30	−0.15	−0.11	0.08
GKD357	14.64	−1.27	0.15	−0.07	0.04
Other $PM_{2.5}$ samples in this study[a]	37.96 ± 74.32	−0.67 ± 0.64	−0.34 ± 0.59	−0.44 ± 0.55	0.03 ± 0.04
Non-haze $PM_{2.5}$ samples reported by Huang et al. (2019) [a]	15.15 ± 27.64	−0.58 ± 0.74	0.20 ± 0.64	0.14 ± 0.54	0.14 ± 0.54

[a] The variation ranges of PBM con. and mercury isotopic compositions of $PM_{2.5}$ samples were expressed by mean ± 2 SD.

3.3. Potential sources of elevated $PM_{2.5}$-Hg during the autumn haze period

3.3.1. Autumn haze in 2014

As shown in Fig. 4a, the total ΣPBM emission displayed similar and inverse variations with the contents of PBM and $\Delta^{199}Hg_{PBM}$, respectively, during the autumn haze period (lasted for five days) in 2014, indicating that anthropogenic emission sources had contributed to the elevated PBM during this period. It was found that the contents of NO_3^-, NH_4^+, and Cl^- had similar variations, which all contained a generally rise-decline trend in this haze period (Figure S3). Since these water-soluble ions may have connection with specific anthropogenic emission sources (Hu et al., 2014), the results may indicate the anthropogenic contribution during this period again. The correlation between fractional ΣPBM emission and $\Delta^{199}Hg_{PBM}$ in the aerosol samples collected during the haze period is shown in Fig. 5, which shows that the fractional ΣPBM emission from northern China had significantly negative correlations with $\Delta^{199}Hg_{PBM}$ in aerosol samples collected during this period ($r = -0.82$, $p = 0.02$). This suggests that air masses with high exposure to the anthropogenic emission sources of northern China may be responsible for the negative shift in $\Delta^{199}Hg_{PBM}$. It was found that the transmission heights of PBM emitted by anthropogenic emission sources in northern China mostly ranged from 0 to 500 m in the autumn of 2014, indicating transport in the PBL (Figure S4). The transport duration times ranged from 0 to 48 h in this haze period (Figure S5). It was assumed that the PBM emitted by anthropogenic emission sources in northern China was unlikely to have been strongly impacted by photoreduction, since it was transported quickly in the PBL and lower free troposphere (Fu et al., 2019). This could cause the Δ^{199}Hg of the PBM emitted by anthropogenic emission sources in northern China to be similar to that of the original anthropogenic emissions (i.e., negative or approximately zero) when transported to the sampling sites (Fu et al., 2019). According to Fig. 5a, the $\Delta^{199}Hg_{PBM}$ of the aerosol samples collected during the 2014 autumn haze period ranged from −0.02% to −0.37%, which was within the ranges of coal combustion, metal smelting, cement production, road dust, and topsoil (Huang et al., 2016; Sun et al., 2013, 2014). It was discovered that the fractional ΣPBM emission from northern China also exhibited similar and inverse variations with the contents of PBM and $\Delta^{199}Hg_{PBM}$, respectively, during this haze period. This suggested that coal combustion, metal smelting, cement production, road dust, and topsoil from northern China provided important contributions to the elevated PBM during this haze period.

In this period, the fractional ΣPBM emissions of other regions of China basically remained constant during the early period and decreased significantly during the later period, a pattern which may indicate that the anthropogenic emission sources from other regions of

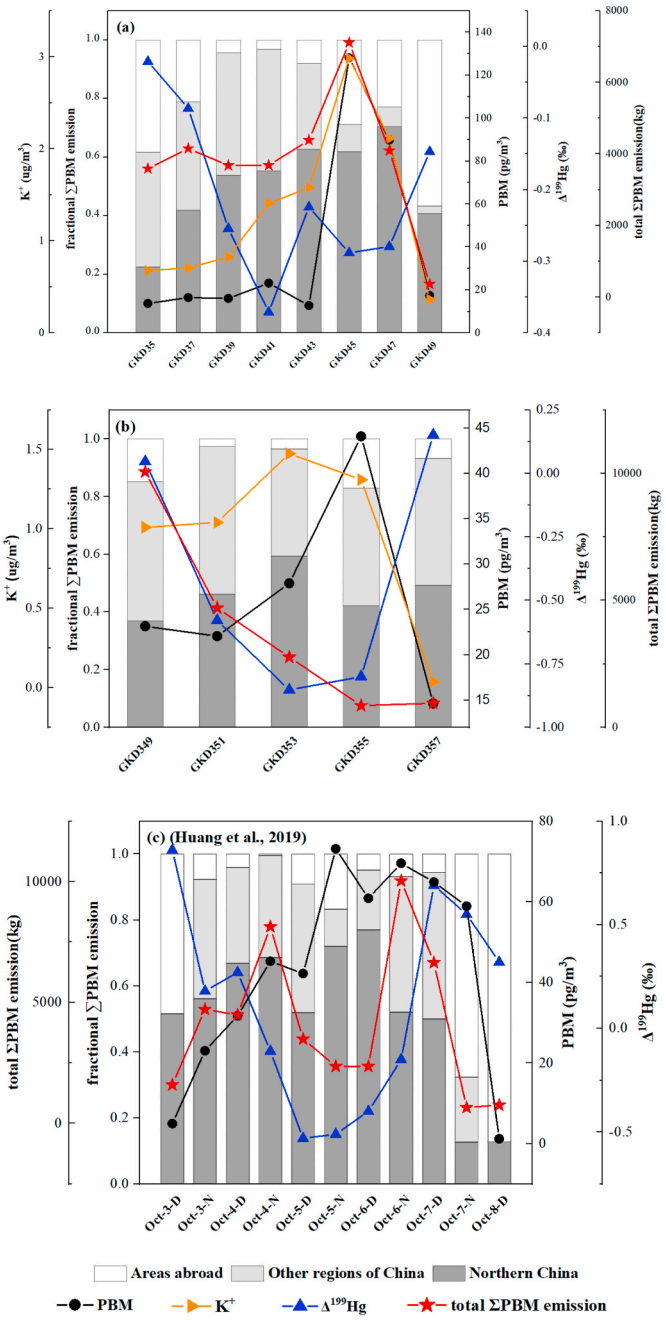

Fig. 4. **(a)** Variation of total and fractional ΣPBM emission, content of K^+, $\Delta^{199}Hg_{PBM}$, and content of PBM in a haze case in autumn in 2014. **(b)** Variation of total and fractional ΣPBM emission, content of K^+, $\Delta^{199}Hg_{PBM}$, and content of PBM in a haze case in winter in 2014. **(c)** Variation of total and fractional ΣPBM emission, $\Delta^{199}Hg_{PBM}$, and content of PBM in a haze case in autumn in 2015 ($\Delta^{199}Hg_{PBM}$ data was reported by Huang et al. (2019)).

China contributed little to the elevated PBM during the haze period. According to Fig. 5, the fractional ΣPBM emissions from other regions of China exhibited no correlation with $\Delta^{199}Hg_{PBM}$ during the autumn of 2014 ($r = 0.31$, $p = 0.50$). For the aerosol samples collected in this haze period, the backward trajectories of the air masses could be divided into two directions, north and northwest. It was found that the north and northwest air masses mainly passed through northeastern Inner Mongolia and the northern Xinjiang region of China (Figure S6). Moreover, the transmission height and transport duration times of the PBM emitted by anthropogenic emission sources in northeastern Inner Mongolia ranged from 0 to 3 km and 96–120 h, respectively, while the

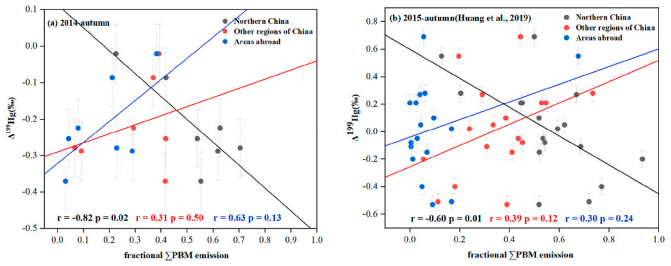

Fig. 5. **(a)** Correlation between the fractional ΣPBM emission of different regions and $\Delta^{199}Hg_{PBM}$ in Beijing in autumn in 2014. **(b)** Correlation between fractional ΣPBM emission of different regions and $\Delta^{199}Hg_{PBM}$ in Beijing in autumn in 2015 ($\Delta^{199}Hg_{PBM}$ data was reported by Huang et al. (2019)). The uncertainty of each sample was expressed as 2 SD.

corresponding values for northern Xinjiang were 3–4 km and 24–72 h, respectively (Figures S4 and S5). Thus, it was found that the transport duration times of the PBM emitted by anthropogenic emission sources in these two regions were different, which may have resulted in different transformation intensities of the PBM emitted by the anthropogenic emission sources in these regions due to photoreduction (Ariya et al., 2015). The mixing of air masses containing the PBM emitted by anthropogenic emission sources in these regions may have led to a poor correlation between the fractional ΣPBM emissions of other regions of China and $\Delta^{199}Hg_{PBM}$ during this haze period.

In addition, it was found that the omission of biofuel production and combustion (anthropogenic biomass burning) in the global Hg assessment report published by UNEP in 2013 was another explanation for the poor correlation between the fractional ΣPBM emissions from other regions of China and $\Delta^{199}Hg_{PBM}$ in the 2014 haze period. A previous case study reported that strong contribution from biomass burning was one of the main sources of PBM in Beijing in autumn (Huang et al., 2016). As is well known, fire maps can qualitatively indicate the intensity of biomass burning in different regions. The air-mass backward trajectory of the aerosol samples collected during the haze period in the autumn of 2014 had apparently passed through the fire areas in other regions of China (mainly northeastern China); thus, it was possible that biomass burning had contributed to the PBM of the samples. Based on previous studies, K^+ was considered to represent the contribution of biomass burning. As seen in Fig. 6, the contents of K^+ and PBM exhibited a significantly positive correlation ($r = 0.91$, $p < 0.01$) in the aerosol samples collected during the haze period in the autumn of 2014, further demonstrating that biomass burning contributed to the sample PBM at that time. As seen in Fig. 4a, the K^+ content was found to display similar and inverse variations with the PBM content and $\Delta^{199}Hg_{PBM}$, respectively. According to the above analysis, biomass burning in other regions of China (mainly northeastern China) may have contributed to the PBM in the aerosol samples collected during the haze period in the autumn of 2014, indicating that biomass burning in northeastern China contributed to the elevated PBM in this haze period.

The fractional ΣPBM emissions of long-range transport exhibited similar and inverse variations with $\Delta^{199}Hg_{PBM}$ and PBM content, respectively, during the autumn 2014 haze period. According to the transmission heights and transport duration times of the air-mass backward trajectories, the transmission heights and duration times of the anthropogenic emission sources from long-range transport ranged from 2 to 5 km and 48–120 h, respectively. Therefore, the PBM emitted by the long-range anthropogenic emission sources was transported through the middle-low free troposphere and experienced a relatively long transport duration time, resulting in a positive $\Delta^{199}Hg_{PBM}$ shift due to the strong effect of photoreduction. The latest global PBM emission inventory reported the grid data of total anthropogenic emissions in 2010 (published in 2013), whereas the sampling of the aerosol samples collected during the autumn haze in this study occurred in 2014. The amount of PBM emitted by anthropogenic emission sources of long-

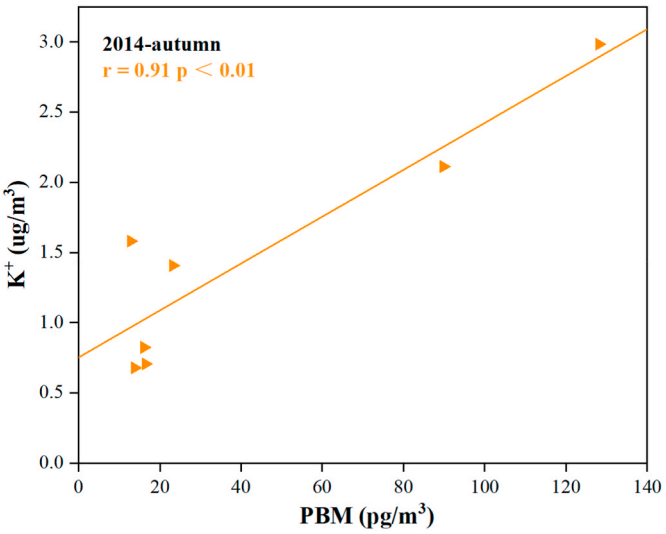

Fig. 6. Correlation between the content of K^+ and PBM in the aerosol samples collected during the 2014 autumn haze period in Beijing.

range transport in 2014 (actual sampling time) was likely to be different than the amount in 2010, and this difference was likely a cause of the non-significant positive correlation between the fractional ΣPBM emissions of long-range transport and $\Delta^{199}Hg_{PBM}$ in the aerosol samples collected during the haze period in the autumn of 2014.

It was shown that the fractional ΣPBM emissions from long-range transport displayed an inverse variation with PBM content, indicating the possibility that the anthropogenic emission sources of long-range transport contributed little to the elevated PBM during this haze period (even playing the role of haze "dilutor"). As shown in Fig. 3 and A3, the air-mass backward trajectories of the aerosol samples collected during this haze period mainly came from two directions, north and northwest, and the PBM emitted by the anthropogenic emission sources of the long-range transport was much less than that of China in these directions. Therefore, according to the calculation formula for fractional ΣPBM emission, the total ΣPBM emission was relatively low when the fractional ΣPBM emissions of long-range transport were high, indicating that the samples were relatively "clean," i.e., the content of PBM in the samples was close to the background value. Hence, the increasing fractional ΣPBM emissions of long-range transport at the end of the haze period may indicate that the PBM content in the sampling sites "recovered" to the background value. According to Huang et al. (2016), the $\Delta^{199}Hg_{PBM}$ of the background total suspended particle (TSP) sample collected from the Yanqing region was 0.18‰, which was higher than that of the $PM_{2.5}$ samples collected simultaneously in the center of Beijing. In this study, the $\Delta^{199}Hg_{PBM}$ of the $PM_{2.5}$ sample collected at the end of the haze period (GKD49) was −0.15‰, which was much lower than 0.18‰. This may indicate that the $\Delta^{199}Hg_{PBM}$ of the baseline $PM_{2.5}$ in the center of Beijing was still lower than that of the long-range transport in adjacent rural regions, although it was higher than that of the $PM_{2.5}$ samples collected during the haze period, indicating a likely anthropogenic impact.

In general, anthropogenic emission sources from northern China and biomass burning in northeastern China jointly contributed to the elevated PBM in the autumn 2014 haze period. According to Fig. 7, there was a significantly negative correlation between $\delta^{202}Hg_{PBM}$ and PBM^{-1} during this haze period, indicating that PBM was mainly controlled by two end members in this period (Estrade et al., 2011). According to the analysis above, this was interpreted to suggest that the mixture of coal combustion, metal smelting, cement production, road dust, and topsoil and other anthropogenic emission sources from northern China and biomass burning in northeastern China represented the polluted end member, whereas the atmospheric background PBM represented the clean end member.

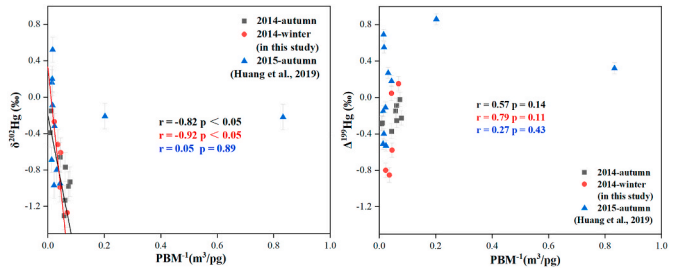

Fig. 7. (a) Correlation between $\delta^{202}Hg_{PBM}$ and PBM^{-1} during the haze period in Beijing in autumn and winter ($\delta^{202}Hg_{PBM}$ data in the autumn of 2015 was reported by Huang et al., 2019). **(b)** Correlation between $\Delta^{199}Hg_{PBM}$ and PBM^{-1} during the haze period in Beijing in autumn and winter ($\Delta^{199}Hg_{PBM}$ data in the autumn of 2015 was reported by Huang et al., 2019). The uncertainty of each sample was expressed as 2 SD.

3.3.2. *Autumn haze in 2015*

As can be seen in Fig. 4c, total ΣPBM emission exhibited similar variation with the PBM content during the early and later stages of the autumn 2015 haze period (lasted for six days), which may indicate the likelihood that anthropogenic emission sources had contributed to the elevated PBM at those times. Moreover, total ΣPBM emission exhibited inverse variation with $\Delta^{199}Hg_{PBM}$ just during the early stage of this haze period. Given the signature of $\Delta^{199}Hg$ in PBM emitted by anthropogenic emission sources (negative or close to zero), it may mean that there had other emission sources contributed to the elevated PBM in this haze period besides anthropogenic emissions. As shown in Fig. 5, the fractional ΣPBM emission from northern China had significantly negative correlations with $\Delta^{199}Hg_{PBM}$ in aerosol samples collected during this haze period ($r = -0.60$, $p = 0.01$). It was found that the transmission heights of PBM emitted by anthropogenic emission sources in northern China ranged from 0 to 3 km (mostly > 500 m) in the autumn of 2015 (Figure S4), indicating primarily transport at a height between the PBL and lower free troposphere. The transport duration times ranged from 0 to 48 h in this haze period (Figure S5). Since the correlation between fractional ΣPBM emission from northern China and $\Delta^{199}Hg_{PBM}$ of the autumn haze in 2015 was weaker than that of the autumn haze in 2014, and the range of $\Delta^{199}Hg_{PBM}$ in the aerosol samples collected during the haze period in 2015 (−0.53‰–0.69‰, 1 SD = 0.34‰) was larger than that in 2014 (−0.37‰ to −0.02‰, 1 SD = 0.12‰), it was speculated that there were other sources besides the sources mentioned in the analysis of the 2014 autumn haze and/or pathways (e.g., photoreduction) contributing to the elevated PBM during this haze period (Huang et al., 2019). Moreover, the transport height of air masses emitted by emission sources in northern China during the autumn haze in 2014 was mostly less than 500 m, whereas that in 2015 was mostly higher than 500 m. Considering the effect of photoreduction on $\Delta^{199}Hg_{PBM}$, this may indicate that PBM was more susceptible to photoreduction when transported at a height over 500 m.

Since the air-mass backward trajectories of aerosol samples collected during the haze period in the autumn of 2015 passed through fire areas in other regions of China (mainly eastern China), based on the analysis above, the omission of anthropogenic biomass burning (see the global Hg assessment report published by UNEP in 2013) might also account for the non-significant positive correlation between the fractional ΣPBM emissions from other regions of China and $\Delta^{199}Hg_{PBM}$ in the aerosol samples collected during the haze period in the autumn of 2015 ($r = 0.39$, $p = 0.12$). Generally, natural vegetation materials have slightly negative $\Delta^{199}Hg$ (Blum et al., 2014).

The fractional ΣPBM emissions of long-range transport exhibited no correlation with $\Delta^{199}Hg_{PBM}$ in aerosol samples collected during the haze period in the autumn of 2015 ($r = 0.30$, $p = 0.24$). The fractional ΣPBM

emissions of long-range transport in all the aerosol samples, except one collected during the 2015 autumn haze, were found to be < 0.2, indicating the small contribution of anthropogenic emission sources in the long-range transport to the PBM sample. According to the analysis above, the omission of anthropogenic biomass burning in the global Hg assessment report published by UNEP in 2013 might also account for the poor correlation between the fractional ΣPBM emissions of the long-range transport and $\Delta^{199}Hg_{PBM}$ in the aerosol samples collected during the 2015 autumn haze.

The total ΣPBM emission maintained a low level during the intermediate stage of the haze period, indicating that there were contributions from other sources to the elevated PBM during this stage. Based on the analysis above, it was speculated that biomass burning may be one of the sources that contributed to the elevated PBM during the intermediate stage of this haze period. Huang et al. (2016) already identified the clear contribution of biomass burning to the autumn PBM in Beijing, based on a large data set of Hg isotopes and other geochemical parameters. Therefore, the biomass burning in eastern China may have contributed to the elevated PBM during this haze period, although this contribution could not be evaluated more accurately owing to a lack of water-soluble K^+ data (Figure S6).

In general, anthropogenic emission sources from northern China and biomass burning in eastern China contributed to the elevated PBM during the autumn 2015 haze period. As seen in Fig. 7, there was no significant correlation between $\delta^{202}Hg_{PBM}$ and PBM^{-1} in the aerosol samples collected during this haze period, revealing that emission sources contributed to the elevated PBM during this haze period other than these sources. According to the analysis regarding the autumn 2014 and 2015 haze period, biomass burning (mainly anthropogenic) also played an important role in the elevated PBM in autumn haze in Beijing in addition to traditional anthropogenic emission sources (e.g., coal combustion, metal smelting, cement production, road dust, and topsoil).

3.4. Potential sources of elevated $PM_{2.5}$-Hg during haze in winter

According to Fig. 4b, the total ΣPBM emission continued to decrease, while the contents of PBM in the aerosol samples exhibited a distinct increase during the haze period (lasted for three days) in the winter of 2014, possibly suggesting that anthropogenic emission sources published in the assessment report did not have a dominant contribution to the elevated PBM in this haze period. It should be pointed out that there need more samples to demonstrate the perspective above based on the limited amounts of samples in this study. According to variations of other water-soluble ions in this haze period (Figure S3), it was found that water-soluble NO_3^-, SO_4^{2-}, NH_4^+, and Cl^- had similar variation trends in the winter haze in 2014, which showed a distinct decline after this haze period. According to previous studies, urban atmospheric sulfate is usually considered as an indicator of stationary emission sources since it is mainly converted by SO_2 emitted from industrial fossil fuel combustion; while the formation of urban atmospheric NO_3^- was related to vehicle emissions. In addition, the formation of these water-soluble ions was suggested to be connected with secondary aerosol reactions in the atmosphere (Yan et al., 2015; Zhang et al., 2016, 2018). Therefore, it may indicate that these emission sources above had contribution to elevated PBM in this haze period. According to previous studies, the negative values of $\Delta^{199}Hg_{PBM} < -0.75‰$ were unlikely to have originated from sources other than biomass burning during this haze period, as most anthropogenic emissions would be characterized by a $\Delta^{199}Hg$ close to zero. Moreover, the K^+ content displayed similar and inverse variations with the contents of PBM and $\Delta^{199}Hg_{PBM}$, respectively, indicating that biomass burning contributed to the elevated PBM in this haze period (Carignan et al., 2009). During the later stage of the winter 2014 haze period, both the K^+ and PBM contents decreased significantly, although the fractional ΣPBM emission of northern China appeared to increase slightly, indicating that the reduction in biomass burning was the main reason for the termination of this haze period. This analysis may indicate that biomass burning played an important role in the elevated PBM, particularly at the early stage of this haze period. It was found that the fire areas that the air-mass backward trajectories passed through were located primarily in northeastern China (Figure S7), indicating that the biomass burning that contributed to the elevated PBM during this haze period may have come primarily from northeastern China.

In general, biomass burning in northeastern China was one of the dominant sources of the elevated PBM during the haze period in the winter of 2014. As shown in Fig. 7, there was a significantly negative correlation between $\delta^{202}Hg_{PBM}$ and PBM^{-1} in the aerosol samples from this haze period, indicating that the aerosol samples in this period were mainly controlled by two end members (Chen et al., 2012; Estrade et al., 2011). Based on the above analysis, it was concluded that the biomass burning in northeastern China would be an important contributing source, as indicated by our data set and air-mass trajectory analysis; meanwhile, the long-range transport from other regions of China, which is generally characterized by higher $\Delta^{199}Hg$, serves as an additional source as the atmospheric background end member.

3.5. Characteristics of $\Delta^{200}Hg_{PBM}$ and their implications for source identification

According to previous studies, significant differences exist between the $\Delta^{200}Hg$ in precipitation and vapor phase, e.g., the $\Delta^{200}Hg$ of precipitation samples is positive, whereas that of the vapor-phase samples is either negative or approximately zero (Chen et al., 2012; Demers et al., 2013; Gratz et al., 2010; Wang et al., 2015). Chen et al. (2012) reported the significant positive Δ200Hg (up to 1.24‰) in precipitation samples collected in Peterborough, ON, Canada. It was found that whatever the movements of air masses in near surface layers, all cold samples with a significant positive $\Delta^{200}Hg$ displayed a downward transport of air mass from more than 6000 m AGL in the arctic region to the near surface layer (500 m AGL), while moving southward to Peterborough. Since the troposphere was shallower near the North Pole (i.e. 6000 m) (Holton et al., 1995; James et al., 2003; Stohl et al., 2003), this may suggest that the significant positive $\Delta^{200}Hg$ in Hg^{2+} in precipitation samples is triggered by processes occurred during the invasion of air mass from stratosphere to troposphere. In addition, the $\Delta^{200}Hg$ of the precipitation samples gradually increases with elevated latitude (Wang et al., 2015), given the research results in Chen et al. (2012), this phenomenon could be explained that the invasion of air mass from stratosphere to troposphere would become more difficult as the troposphere was deeper in the subtropical regions. It may indicate that the process that triggers the generation of $\Delta^{200}Hg$ is more likely to occur in the upper troposphere. Moreover, previous studies have established a conceptual model for the generation of $\Delta^{200}Hg$ in the precipitation samples (Cai and Chen, 2016; Chen et al., 2012). According to previous studies, PBM samples and water vapor samples exhibited similar differences in $\Delta^{200}Hg$, indicating that the conceptual model may also apply to the PBM samples (Rolison et al., 2013). Therefore, $\Delta^{200}Hg_{PBM}$ was considered to be an indicator of the transport of PBM from the upper troposphere to the surface, if, in fact, the conceptual model proposed by Chen et al. (2012) is valid.

If $\Delta^{200}Hg_{PBM}$ only indicated the contribution of PBM generated by photo-initiated oxidation on aerosols or solid surfaces in the upper troposphere, it would have no correlation with the anthropogenic emissions. As seen in Fig. 8, although there was no correlation between $\Delta^{200}Hg_{PBM}$ and fractional ΣPBM emissions of different regions during the haze periods in the autumn and winter of 2014, there were significant correlations ($p < 0.05$) between $\Delta^{200}Hg_{PBM}$ and the fractional ΣPBM emissions of different regions during the haze period in the autumn of 2015, indicating that the $\Delta^{200}Hg_{PBM}$ found in these samples would be somehow related to anthropogenic emissions, although the mechanism is unclear. In addition, the proportions of the frequencies of various height ranges of air-mass backward trajectories were calculated for the three haze periods. As seen in Fig. 9, there had uncorrelated

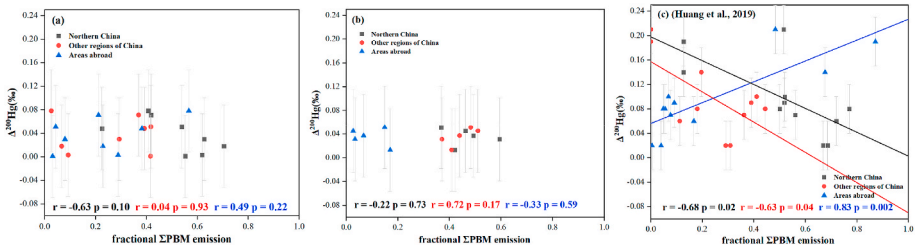

Fig. 8. (a) Correlation between fractional ΣPBM emission of different regions and $\Delta^{200}Hg_{PBM}$ in the haze period in the autumn of 2014. **(b)** Correlation between fractional ΣPBM emission of different regions and $\Delta^{200}Hg_{PBM}$ in the haze period in the winter of 2014. **(c)** Correlation between fractional ΣPBM emission of different regions and $\Delta^{200}Hg_{PBM}$ in the haze period in the autumn of 2015 ($\Delta^{200}Hg_{PBM}$ data in the autumn of 2015 was reported by Huang et al. (2019)). The uncertainty of each sample was expressed as 2 SD.

variation between $\Delta^{200}Hg_{PBM}$ and the proportions of height range frequencies (>5 km) of air-mass backward trajectories during the 2014 autumn haze period, whereas an inverse variation existed between them during the other two haze periods, possibly revealing that $\Delta^{200}Hg_{PBM}$ may have other contributors, in addition to the PBM transported from the upper troposphere. Therefore, it was suggested that PBM partially generated by photo-initiated oxidation on aerosols (e.g. the surface layer of frozen water droplets) and/or solid surfaces (e.g. snow crystals, new-formed compounds of Hg) in the upper troposphere (Chen et al., 2012) and that emitted by anthropogenic emission sources might both contribute to $\Delta^{200}Hg_{PBM}$. Au Yang et al. (2019) demonstrated that heterogeneous photoreactions on mineral dust would be another oxidation pathway to induce $\Delta^{33}S$. Our observation suggests such an additional Hg^0 oxidation process in the presence of aerosols, triggering $\Delta^{200}Hg$ in the product Hg species; however, the exact mechanisms need to be deeply investigated. The emissions from various sectors are listed in Table S6, which shows that artisanal and small-scale gold mining (37%), coal burning (24%), primary production of nonferrous metals (Cu, Pb, Zn) (10%), and cement production (9%) generally comprised the largest proportions of anthropogenic emissions to global atmospheric PBM. It was found that the variation trend of Cu and Pb was similar to that of PBM in the autumn haze period in 2014, while the contents of Cu, Pb, and PBM all had a distinct decline after the winter haze period in 2014 (Figure S8), which may further confirm the contributions of primary production of nonferrous metals and cement production. Because there was not a considerable number of gold mines around Beijing, the contribution of artisanal and small-scale gold mining to elevated PBM during the haze periods in Beijing would be limited. Therefore, coal burning, primary production of nonferrous metals (Cu, Pb, Zn), and cement production are more likely to be the anthropogenic emission sources that contribute to the $\Delta^{200}Hg_{PBM}$ of PBM. Given the above analysis, the indication function of $\Delta^{200}Hg_{PBM}$ should be explored in future research, since only three haze periods were investigated in this study and more samples are needed to demonstrate the accuracy of this speculation.

4. Conclusions

In this study, the potential sources and source regions of PBM during haze periods were identified using Hg isotopes combined with air-mass trajectory analysis. The $\Delta^{199}Hg_{PBM}$ was found to be a good tracer for identifying the potential sources and transport of PBM, although it is adversely affected by uncertainties. It is speculated that the indication function of $\Delta^{199}Hg_{PBM}$ would be more distinct if the accuracy of the anthropogenic emission inventory were improved (especially through the addition of the anthropogenic biomass burning sector). In addition, anthropogenic emission sources, including coal combustion, metal smelting, cement production, road dust, and topsoil from northern China and biomass burning (especially in northeastern China), were found to considerably contribute to elevated PBM during the haze periods. Based on previous studies, $\Delta^{200}Hg_{PBM}$ was considered to be a good tracer for PBM generated by photo-initiated oxidation on aerosols or solid surfaces in the upper troposphere; meanwhile, anthropogenic emission sources, which include coal burning, primary production of nonferrous metals (Cu, Pb, Zn), and cement production, may also have contributed to the $\Delta^{200}Hg_{PBM}$ in this study through heterogeneous photoreactions on these emitted particles. These results show that the indication function of $\Delta^{200}Hg_{PBM}$ requires additional research to confirm its validity.

CRediT authorship contribution statement

Yue Qiu: Conceptualization, Formal analysis, Investigation, Visualization, Writing - original draft. **Pengxue Gai:** Investigation. **Fange Yue:** Investigation, Resources. **Yuanyuan Zhang:** Investigation. **Pengzhen He:** Investigation, Resources. **Hui Kang:** Resources. **Xiawei Yu:** Visualization, Resources. **Paul K.S. Lam:** Writing - review & editing. **Jiubin Chen:** Writing - review & editing, Project administration, Funding acquisition. **Zhouqing Xie:** Conceptualization, Writing - review & editing, Supervision, Project administration, Funding acquisition.

Declaration of competing interest

The authors declare that they have no known competing financial

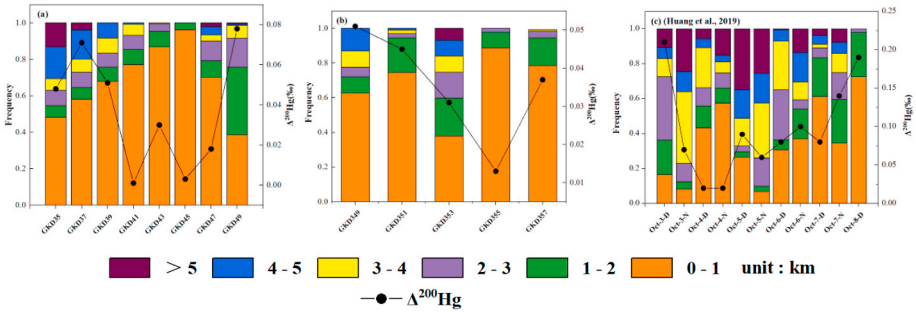

Fig. 9. (a) Variation of frequency of height ranges of air-mass backward trajectory and $\Delta^{200}Hg_{PBM}$ in the haze period in the autumn of 2014. **(b)** Variation of frequency of height ranges of air-mass backward trajectory and $\Delta^{200}Hg_{PBM}$ in the haze period in the winter of 2014. **(c)** Variation of frequency of height ranges of air-mass backward trajectory and $\Delta^{200}Hg_{PBM}$ in the haze period in the autumn of 2015. ($\Delta^{200}Hg_{PBM}$ data in the autumn of 2015 was reported by Huang et al. (2019)).

interests or personal relationships that could have appeared to influence the work reported in this paper.

Acknowledgments

This work was supported by the National Key Project of Ministry of Science and Technology of China (2016YFC0203302), the National Natural Science Foundation of China (Nos. 91544103), and the National Natural Science Foundation of China (Nos. 41830647, 41625012, 41961144028). We would like to thank Xuewu Fu for his guide in research methods. We would also like to thank Jianfeng Liu for his assistance in corresponding experiments.

Appendix A. Supplementary data

Supplementary data to this article can be found online at https://doi.org/10.1016/j.atmosenv.2021.118203.

References

AMAP/UNEP, 2013. Geospatially Distributed Mercury Emissions Dataset 2010 v1. dataset.

Andreae, M.O., 2019. Emission of trace gases and aerosols from biomass burning - an updated assessment. Atmos. Chem. Phys. 19, 8523–8546. https://doi.org/10.5194/acp-19-8523-2019.

Archer, D.E., Blum, J.D., 2018. A model of mercury cycling and isotopic fractionation in the ocean. Biogeosciences 15, 6297–6313. https://doi.org/10.5194/bg-15-6297-2018.

Ariya, P.A., Amyot, M., Dastoor, A., Deeds, D., Feinberg, A., Kos, G., Poulain, A., Ryjkov, A., Semeniuk, K., Subir, M., Toyota, K., 2015. Mercury physicochemical and biogeochemical transformation in the atmosphere and at atmospheric interfaces: a review and future directions. Chem. Rev. 115, 3760–3802. https://doi.org/10.1021/cr500667e.

Bergquist, B.A., Blum, J.D., 2007. Mass-dependent and -independent fractionation of Hg isotopes by photoreduction in aquatic systems. Science 318, 417–420. https://doi.org/10.1126/science.1148050.

Cai, H., Chen, J., 2016. Mass-independent fractionation of even mercury isotopes. Sci. Bull. 61, 116–124. https://doi.org/10.1007/s11434-015-0968-8.

Carignan, J., Estrade, N., Sonke, J.E., Donard, O.F.X., 2009. Odd isotope deficits in atmospheric Hg measured in lichens. Environ. Sci. Technol. 43, 5660–5664. https://doi.org/10.1021/es900578v.

Chen, J., Hintelmann, H., Dimock, B., 2010. Chromatographic pre-concentration of Hg from dilute aqueous solutions for isotopic measurement by MC-ICP-MS. J. Anal. At. Spectrom. 25, 1402–1409. https://doi.org/10.1039/c0ja00014k.

Chen, J., Hintelmann, H., Feng, X., Dimock, B., 2012. Unusual fractionation of both odd and even mercury isotopes in precipitation from Peterborough, ON, Canada. Geochem. Cosmochim. Acta 90, 33–46. https://doi.org/10.1016/j.gca.2012.05.005.

Chen, Q., Geng, L., Schmidt, J.A., Xie, Z., Kang, H., Dachs, J., Cole-Dai, J., Schauer, A.J., Camp, M.G., Alexander, B., 2016. Isotopic constraints on the role of hypohalous acids in sulfate aerosol formation in the remote marine boundary layer. Atmos. Chem. Phys. 16, 11433–11450. https://doi.org/10.5194/acp-16-11433-2016.

Cheng, Y., Engling, G., He, K., Duan, F., Ma, Y., Du, Z., Liu, J., Zheng, M., Weber, R.J., 2013. Biomass burning contribution to Beijing aerosol. Atmos. Chem. Phys. 13, 7765–7781. https://doi.org/10.5194/acp-13-7765-2013.

Cheng, I., Xu, X., Zhang, L., 2015. Overview of receptor-based source apportionment studies for speciated atmospheric mercury. Atmos. Chem. Phys. 15, 7877–7895. https://doi.org/10.5194/acp-15-7877-2015.

Cui, Y., Ji, D., He, J., Kong, S., Wang, Y., 2020. In situ continuous observation of hourly elements in PM2.5 in urban beijing, China: occurrence levels, temporal variation, potential source regions and health risks. Atmos. Environ. 222, 11. https://doi.org/10.1016/j.atmosenv.2019.117164.

Chylek, P., Zhan, J., 1990. Absorption and scattering OF light BY small particles - the interference structure. Appl. Optic. 29 https://doi.org/10.1364/ao.29.003984, 3984-3984.

Demers, J.D., Blum, J.D., Zak, D.R., 2013. Mercury isotopes in a forested ecosystem: implications for air-surface exchange dynamics and the global mercury cycle. Global Biogeochem. Cycles 27, 222–238. https://doi.org/10.1002/gbc.20021.

Dibb, J.E., Talbot, R.W., Whitlow, S.I., Shipham, M.C., Winterle, J., McConnell, J., Bales, R., 1996. Biomass burning signatures in the atmosphere and snow at Summit, Greenland: an event on 5 August 1994. Atmos. Environ. 30, 553–561. https://doi.org/10.1016/1352-2310(95)00328-2.

Duan, L., Xiu, G., Feng, L., Cheng, N., Wang, C., 2016. The mercury species and their association with carbonaceous compositions, bromine and iodine in PM2.5 in Shanghai. Chemosphere 146, 263–271. https://doi.org/10.1016/j.chemosphere.2015.11.058.

Estrade, N., Carignan, J., Donard, O.F.X., 2011. Tracing and quantifying anthropogenic mercury sources in soils of northern France using isotopic signatures. Environ. Sci. Technol. 45, 1235–1242. https://doi.org/10.1021/es1026823.

Estrade, N., Carignan, J., Sonke, J.E., Donard, O.F.X., 2009. Mercury isotope fractionation during liquid-vapor evaporation experiments. Geochem. Cosmochim. Acta 73, 2693–2711. https://doi.org/10.1016/j.gca.2009.01.024.

Fu, X., Feng, X., Sommar, J., Wang, S., 2012. A review of studies on atmospheric mercury in China. Sci. Total Environ. 421, 73–81. https://doi.org/10.1016/j.scitotenv.2011.09.089.

Fu, X., Zhang, H., Feng, X., Tan, Q., Ming, L., Liu, C., Zhang, L., 2019. Domestic and transboundary sources of atmospheric particulate bound mercury in remote areas of China: evidence from mercury isotopes. Environ. Sci. Technol. 53, 1947–1957. https://doi.org/10.1021/acs.est.8b06736.

Gratz, L.E., Keeler, G.J., Blum, J.D., Sherman, L.S., 2010. Isotopic composition and fractionation of mercury in great lakes precipitation and ambient air. Environ. Sci. Technol. 44, 7764–7770. https://doi.org/10.1021/es100383w.

Hintelmann, H., Lu, S., 2003. High precision isotope ratio measurements of mercury isotopes in cinnabar ores using multi-collector inductively coupled plasma mass spectrometry. Analyst 128, 635–639. https://doi.org/10.1039/b300451a.

Holton, J.R., Haynes, P.H., McIntyre, M.E., Douglass, A.R., Rood, R.B., Pfister, L., 1995. Stratosphere-troposphere exchange. Rev. Geophys. 33, 403–439. https://doi.org/10.1029/95RG02097.

Hong, Q., Xie, Z., Liu, C., Wang, F., Xie, P., Kang, H., Xu, J., Wang, J., Wu, F., He, P., Mou, F., Fan, S., Dong, Y., Zhan, H., Yu, X., Chi, X., Liu, J., 2016. Speciated atmospheric mercury on haze and non-haze days in an inland city in China. Atmos. Chem. Phys. 16, 13807–13821. https://doi.org/10.5194/acp-16-13807-2016.

Hu, Q., Zhang, L., Evans, G.J., Yao, X., 2014. Variability of atmospheric ammonia related to potential emission sources in downtown Toronto, Canada. Atmos. Environ. 99, 365–373. https://doi.org/10.1016/j.atmosenv.2014.10.006.

Huang, Q., Liu, Y., Chen, J., Feng, X., Huang, W., Yuan, S., Cai, H., Fu, X., 2015. An improved dual-stage protocol to pre-concentrate mercury from airborne particles for precise isotopic measurement. J. Anal. At. Spectrom. 30, 957–966. https://doi.org/10.1039/c4ja00438h.

Huang, Q., Chen, J., Huang, W., Fu, P., Guinot, B., Feng, X., Shang, L., Wang, Z., Wang, Z., Yuan, S., Cai, H., Wei, L., Yu, B., 2016. Isotopic composition for source identification of mercury in atmospheric fine particles. Atmos. Chem. Phys. 16, 11773–11786. https://doi.org/10.5194/acp-16-11773-2016.

Huang, Q., Chen, J., Huang, W., Reinfelder, J.R., Fu, P., Yuan, S., Wang, Z., Yuan, W., Cai, H., Ren, H., Sun, Y., He, L., 2019. Diel variation in mercury stable isotope ratios records photoreduction of PM2.5-bound mercury. Atmos. Chem. Phys. 19, 315–325. https://doi.org/10.5194/acp-19-315-2019.

James, P., Stohl, A., Forster, C., Eckhardt, S., Seibert, P., Frank, A., 2003. A 15-year climatology of stratosphere-troposphere exchange with a Lagrangian particle dispersion model - 2. Mean climate and seasonal variability. J. Geophys. Res. Atmos. 108, 16. https://doi.org/10.1029/2002jd002639.

Janssen, S.E., Schaefer, J.K., Barkay, T., Reinfelder, J.R., 2016. Fractionation of mercury stable isotopes during microbial methylmercury production by iron- and sulfate-reducing bacteria. Environ. Sci. Technol. 50, 8077–8083. https://doi.org/10.1021/acs.est.6b00854.

Jiskra, M., Wiederhold, J.G., Skyllberg, U., Kronberg, R.M., Hajdas, I., Kretzschmar, R., 2015. Mercury deposition and Re-emission pathways in boreal forest soils investigated with Hg isotope signatures. Environ. Sci. Technol. 49, 7188–7196. https://doi.org/10.1021/acs.est.5b00742.

Kritee, K., Blum, J.D., Johnson, M.W., Bergquist, B.A., Barkay, T., 2007. Mercury stable isotope fractionation during reduction of Hg(II) to Hg(0) by mercury resistant microorganisms. Environ. Sci. Technol. 41, 1889–1895. https://doi.org/10.1021/es062019t.

Liang, B., Li, X., Ma, K., Liang, S., 2019. Pollution characteristics of metal pollutants in PM2.5 and comparison of risk on human health in heating and non-heating seasons in Baoding, China. Ecotox. Environ. Safe. 170, 166–171. https://doi.org/10.1016/j.ecoenv.2018.11.075.

Maher, W., Krikowa, F., Ellwood, M., 2020. Mercury cycling in Australian estuaries and near shore coastal ecosystems: triggers for management. Elementa-Sci. Anthrop. 8, 18. https://doi.org/10.1525/elementa.425.

Pacyna, E.G., Pacyna, J.M., Steenhuisen, F., Wilson, S., 2006. Global anthropogenic mercury emission inventory for 2000. Atmos. Environ. 40, 4048–4063. https://doi.org/10.1016/j.atmosenv.2006.03.041.

Rolison, J.M., Landing, W.M., Luke, W., Cohen, M., Salters, V.J.M., 2013. Isotopic composition of species-specific atmospheric Hg in a coastal environment. Chem. Geol. 336, 37–49. https://doi.org/10.1016/j.chemgeo.2012.10.007.

Rose, C.H., Ghosh, S., Blum, J.D., Bergquist, B.A., 2015. Effects of ultraviolet radiation on mercury isotope fractionation during photo-reduction for inorganic and organic mercury species. Chem. Geol. 405, 102–111. https://doi.org/10.1016/j.chemgeo.2015.02.025.

Selin, N.E., 2009. Global biogeochemical cycling of mercury: a review. Annu. Rev. Environ. Resour. 34, 43–63. https://doi.org/10.1146/annurev.environ.051308.084314.

Sherman, L.S., Blum, J.D., Johnson, K.P., Keeler, G.J., Barres, J.A., Douglas, T.A., 2010. Mass-independent fractionation of mercury isotopes in Arctic snow driven by sunlight. Nat. Geosci. 3, 173–177. https://doi.org/10.1038/ngeo758.

Sherman, L.S., Blum, J.D., Keeler, G.J., Demers, J.D., Dvonch, J.T., 2012. Investigation of local mercury deposition from a coal-fired power plant using mercury isotopes. Environ. Sci. Technol. 46, 382–390. https://doi.org/10.1021/es202793c.

Smith, R.S., Wiederhold, J.G., Kretzschmar, R., 2015. Mercury isotope fractionation during precipitation of metacinnabar (beta-HgS) and montroydite (HgO). Environ. Sci. Technol. 49, 4325–4334. https://doi.org/10.1021/acs.est.5b00409.

Stohl, A., Bonasoni, P., Cristofanelli, P., Collins, W., Feichter, J., Frank, A., Forster, C., Gerasopoulos, E., Gaggeler, H., James, P., Kentarchos, T., Kromp-Kolb, H., Kruger, B., Land, C., Meloen, J., Papayannis, A., Priller, A., Seibert, P., Sprenger, M.,

Roelofs, G.J., Scheel, H.E., Schnabel, C., Siegmund, P., Tobler, L., Trickl, T., Wernli, H., Wirth, V., Zanis, P., Zerefos, C., 2003. Stratosphere-troposphere exchange: a review, and what we have learned from STACCATO. J. Geophys. Res. Atmos. 108, 15. https://doi.org/10.1029/2002jd002490.

Subir, M., Ariya, P.A., Dastoor, A.P., 2012. A review of the sources of uncertainties in atmospheric mercury modeling II. Mercury surface and heterogeneous chemistry - a missing link. Atmos. Environ. 46, 1–10. https://doi.org/10.1016/j.atmosenv.2011.07.047.

Sun, G., Sommar, J., Feng, X., Lin, C., Ge, M., Wang, W., Yin, R., Fu, X., Shang, L., 2016. Mass-dependent and -independent fractionation of mercury isotope during gas-phase oxidation of elemental mercury vapor by atomic Cl and Br. Environ. Sci. Technol. 50, 9232–9241. https://doi.org/10.1021/acs.est.6b01668.

Sun, R., Heimburger, L.E., Sonke, J.E., Liu, G., Amouroux, D., Berail, S., 2013. Mercury stable isotope fractionation in six utility boilers of two large coal-fired power plants. Chem. Geol. 336, 103–111. https://doi.org/10.1016/j.chemgeo.2012.10.055.

Sun, R., Sonke, J.E., Heimburger, L.E., Belkin, H.E., Liu, G., Shome, D., Cukrowska, E., Liousse, C., Pokrovsky, O.S., Streets, D.G., 2014. Mercury stable isotope signatures of world coal deposits and historical coal combustion emissions. Environ. Sci. Technol. 48, 7660–7668. https://doi.org/10.1021/es501208a.

Teng, X., Liu, F.-p., Chiu, Y.-h., 2020. The impact of coal and non-coal consumption on China's energy performance improvement. Nat. Resour. Forum 1–19. https://doi.org/10.1111/1477-8947.12207.

UNEP, 2013. Global Mercury Assessment 2013: Sources, Emissions, Releases and Environmental Transport. UNEP Chemicals Branch, Geneva, Switzerland.

Wang, Z., Chen, J., Feng, X., Hintelmann, H., Yuan, S., Cai, H., Huang, Q., Wang, S., Wang, F., 2015. Mass-dependent and mass-independent fractionation of mercury isotopes in precipitation from Guiyang, SW China. C. R. Geosci. 347, 358–367. https://doi.org/10.1016/j.crte.2015.02.006.

Wang, Q., Wang, L., Li, X., Xin, J., Liu, Z., Sun, Y., Liu, J., Zhang, Y., Du, W., Jin, X., Zhang, T., Liu, S., Liu, Q., Chen, J., Cheng, M., Wang, Y., 2020. Emission characteristics of size distribution, chemical composition and light absorption of particles from field-scale crop residue burning in Northeast China. Sci. Total Environ. 710, 13. https://doi.org/10.1016/j.scitotenv.2019.136304.

Wiederhold, J.G., Cramer, C.J., Daniel, K., Infante, I., Bourdon, B., Kretzschmar, R., 2010. Equilibrium mercury isotope fractionation between dissolved Hg(II) species and thiol-bound Hg. Environ. Sci. Technol. 44, 4191–4197. https://doi.org/10.1021/es100205t.

Yan, J., Chen, L., Lin, Q., Li, Z., Chen, H., Zhao, S., 2015. Chemical characteristics of submicron aerosol particles during a long-lasting haze episode in Xiamen, China. Atmos. Environ. Times 113, 118–126. https://doi.org/10.1016/j.atmosenv.2015.05.003.

Yang, D.A., Cartigny, P., Desboeufs, K., Widory, D., 2019. Seasonality in the Delta S-33 measured in urban aerosols highlights an additional oxidation pathway for atmospheric SO2. Atmos. Chem. Phys. 19, 3779–3796. https://doi.org/10.5194/acp-19-3779-2019.

Yin, R., Feng, X., Meng, B., 2013. Stable mercury isotope variation in rice plants (Oryza sativa L.) from the wanshan mercury mining district, SW China. Environ. Sci. Technol. 47, 2238–2245. https://doi.org/10.1021/es304302a.

Yuan, S., Zhang, Y., Chen, J., Kang, S., Zhang, J., Feng, X., Cai, H., Wang, Z., Wang, Z., Huang, Q., 2015. Large variation of mercury isotope composition during a single precipitation event at Lhasa City, Tibetan Plateau, China. In: Millot, R., Negrel, P. (Eds.), 11th Applied Isotope Geochemistry Conference Aig-11. Elsevier Science Bv, Amsterdam, pp. 282–286. https://doi.org/10.1016/j.proeps.2015.07.066.

Zhang, L., Wang, S., Wang, L., Wu, Y., Duan, L., Wu, Q., Wang, F., Yang, M., Yang, H., Hao, J., Liu, X., 2015. Updated emission inventories for speciated atmospheric mercury from anthropogenic sources in China. Environ. Sci. Technol. 49, 3185–3194. https://doi.org/10.1021/es504840m.

Zhang, Y., Huang, W., Cai, T., Fang, D., Wang, Y., Song, J., Hu, M., Zhang, Y., 2016. Concentrations and chemical compositions of fine particles (PM2.5) during haze and non-haze days in Beijing. Atmos. Res. 174, 62–69. https://doi.org/10.1016/j.atmosres.2016.02.003.

Zhang, R., Sun, X., Shi, A., Huang, Y., Yan, J., Nie, T., Yan, X., Li, X., 2018. Secondary inorganic aerosols formation during haze episodes at an urban site in Beijing, China. Atmos. Environ. 177, 275–282. https://doi.org/10.1016/j.atmosenv.2017.12.031.

Zheng, W., Hintelmann, H., 2009. Mercury isotope fractionation during photoreduction in natural water is controlled by its Hg/DOC ratio. Geochem. Cosmochim. Acta 73, 6704–6715. https://doi.org/10.1016/j.gca.2009.08.016.

Zheng, W., Hintelmann, H., 2010. Isotope fractionation of mercury during its photochemical reduction by low-molecular-weight organic compounds. J. Phys. Chem. 114, 4246–4253. https://doi.org/10.1021/jp9111348.